Superalloys 2012: 12th International Symposium on Superalloys
Edited by: Eric S. Huron, Roger C. Reed, Mark C. Hardy, Michael J. Mills, Rick E. Montero, Pedro D. Portella, Jack Telesman
TMS (The Minerals, Metals & Materials Society), 2012

Residual stress evolution during the manufacture of aerospace forgings.

J. Rolph[1] M. Preuss[1] N. Iqbal[1] M. Hofmann[2] S. Nikov[3] M. C. Hardy[3] M. G. Glavicic[4] R. Ramanathan[5] A. Evans[6]
[1] Materials Science Centre, University of Manchester, Grosvenor St, Manchester, M13 9PL, UK
[2] Forschungs-Neutronenquelle Heinz Maier-Leibnitz (FRM II), TU München, Lichtenbergstsr. 1, 85747 Garching, Germany
[3] Rolls-Royce plc, PO Box 31, Moor Lane, Derby, DE24 8BJ, UK
[4]Rolls-Royce Corporation, Indianapolis, IN, USA
[5] ATI Ladish Forging, 5481 S. Packard Avenue, Cudahy, WI, 53110-8902, USA
[6] Institut Laue-Langevin, 6 rue Jules-Horowitz, BP 156, 38042 Grenoble cedex 9, France
Keywords: Residual stress, Nickel superalloy, Neutron diffraction, Contour method, Finite element modelling

Abstract

The residual stresses present through the quenching, ageing, and machining processes in sub-scale forgings of RR1000 have been measured experimentally using neutron diffraction, and the contour method. The forgings, 88.9mm in diameter, and 25.4-50.8mm thickness, were of small enough geometry to allow neutron strain measurement in 3 directions throughout most of the bulk. The contour method was employed successfully to generate a full 2D map of the hoop stress in the as-aged and machined samples. The two experimental data sets have been shown to agree very well. Finite element modelling predictions based on an experimentally derived heat transfer coefficient (HTC) curve allowed further comparison and generated additional data. Agreement between the experimental and simulated data was found to be reasonable with some discrepancy visible in the axial direction. The water quenching process was found to generate peak stresses up to 1400MPa in the hoop and radial direction, which were relaxed by as much as 700MPa through ageing. Material removal by machining had a less significant impact in most cases, relaxing residual stress by 100-200MPa.

1. Introduction

Aero-engine manufacturers seeking to increase turbine power and efficiency traditionally look to utilise higher turbine entry temperatures, and increase compressor discharge temperatures. To cope with the greater demands of such a design, it is now increasingly necessary to employ the next generation of nickel-base superalloys in the hottest sections of the engine. One such disc alloy is RR1000; developed by Rolls-Royce, it has a γ' volume fraction of close to 50 vol.% and typically a tri-modal γ' distribution. The design temperature capability of RR1000 is 1000°K [1]. To achieve the required mechanical performance, which is closely linked to the microstructure of the material, each component is processed using a sequence of forging and heat treatments before being machined in stages to the finished geometry. In disc components, the best mechanical performance is achieved when a fine γ' particle size distribution is produced, which requires fast cooling rates from solution heat treatment. However, this can generate steep thermal gradients resulting in high levels of residual stress, which can be partially relaxed and re-distributed by the ageing and machining processes respectively.

The precise residual stress distribution is of importance to engine manufacturers for two distinct reasons. Firstly, machining processes remove constraint, which cause the component to distort as residual stresses re-distribute to reach a new equilibrium state. If unaccounted for, such distortions can lead to significant re-working of the component, or additional machining operations. Secondly, residual stresses have a direct impact on the performance of a component as they add to the applied stresses during operation. In the case of tensile residual stresses, they can deteriorate fatigue life and are ultimately passed on to component lifing predictions for service [2]. For these reasons, it has become increasingly important to employ validated process models that predict residual stresses during and post manufacture to tailor individual processes and improve the accuracy of lifing predictions.

Model validation on full-scale production parts can only be carried out in a handful of cases due to the high cost and difficulty in measuring large and complex geometries. In addition, large production geometries limit viable measurement techniques to near surface methods such as hole drilling or lab x-ray diffraction, which can only penetrate to a maximum depth of 1-2mm in this material. The hole drilling technique in particular is subject to a higher level of uncertainty once residual stress levels exceed 60% of yield [3]. However, alternative methods such as neutron and high energy synchrotron x-ray diffraction [4, 5] as well as the so-called contour method [6] enable one to measure residual stresses from the near surface to deep inside the component. Furthers details on these residual stress measurement techniques including typical penetration into engineering materials can be found in [7].

In the present study residual stresses have been characterised in the alloy RR1000 using simplified sub-scale disc geometries to represent the quenching, ageing and machining processes of full scale discs. The geometry of the sub-scale disc was designed to allow neutron diffraction measurements deep inside the samples and the application of the contour method technique whilst maintaining similar levels of residual stress to production parts. The experimental residual stress results from neutron diffraction and contour method have been compared with finite element modelling predictions of the residual stress state with a view to improving current process modelling predictions. To date, the only industrially standardised technique available for model validation is that of hole drilling, thus the measurement of bulk residual stress represents an alternative approach to process model validation.

2. Experimental description – Sample preparation

Sample preparation

Three sub-scale forgings of RR1000 were provided by ATI Ladish Forgings. The nominal chemical composition of RR1000 is given in Table 1. Samples 1 (S1) and 2 (S2) had a diameter of 88.9mm, a bore width of 50.8mm and rim width of 25.4mm (Figure 1). Sample 3 (S3) differs dimensionally in being machined on both faces to give a uniform width of 25.4mm.

Table 1: RR1000 nominal composition (wt%)

Alloy	Ni	Cr	Co	Mo	Ti	Al	C	B	Ta	Zr	Hf
RR1000	Bal.	15	18.5	5	3.6	3	0.027	0.015	2	0.06	0.5

In each case, sample processing began with extraction from a large pancake forging at the same radial distance to ensure a closely matched thermo-mechanical history for each part. S1 was then subjected to a sub γ´ solvus heat treatment at 1120°C for 4 hours before being water quenched. S2 was processed identically with the addition of a 16 hour ageing heat treatment at 760°C. S3 was processed as S2 with a follow up machining operation, which removed material from each face of the bore region (Figure 1). Note that the initial sub γ´ solvus heat treatment is assumed to reduce all forging stresses to zero. Therefore all residual stresses analysed in this study are those initiated from the quenching process alone.

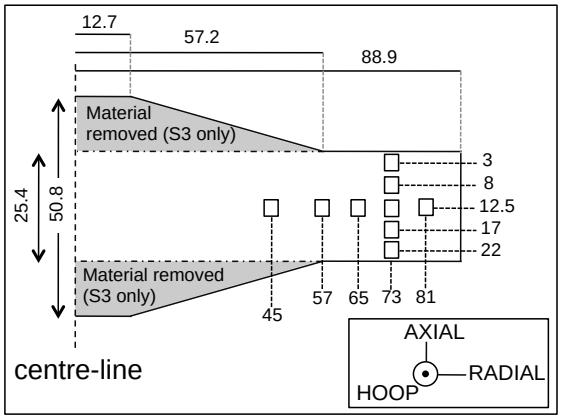

Figure 1: An axi-symmetric cross section of S1, S2, and S3 (with material removal indicated), with neutron diffraction gauge volume locations. All dimensions in mm.

A water quench process was chosen in this sub-scale geometry to achieve high levels of residual stress despite the small geometry of the sample, whilst an ageing temperature of 760°C was chosen because it is a typical stress relief/ageing temperature for γ' strengthened nickel-base superalloys. The machining operation carried out on S3 was designed as a simplified representation of a reduction in cross-section, as carried out in full-scale disc manufacture when moving from heat treatment geometry to finished component.

2.1 Residual stress analysis by neutron diffraction

All neutron diffraction measurements were carried out at the dedicated strain scanning instrument STRESS-SPEC at FRM-II, Germany [8].

Two samples were mounted simultaneously and aligned initially using a computer controlled translator table and theodolite, followed by entry scans with the neutron beam for accurate positioning. The Ni (311) reflection was chosen for the measurement of elastic strain in this alloy as it is known for having low sensitivity to plasticity induced intergranular strains and to exhibit a good representation of bulk behaviour [9]. It is acknowledged however, that in RR1000 the (311) diffraction peak is composed of contributions from both the γ and γ´ phases. The two phases are indistinguishable in most neutron diffraction experiments since they have almost identical lattice parameters; thus a single peak is observed where the two contributions overlap. Measuring bulk strain with a composite peak such as this assumes both the γ and γ´ phases accommodate load without any significant partitioning, which would otherwise alter the peak shape. Throughout peak fitting and analysis, care was taken to ensure peak symmetry was observed and the Gaussian fit could be applied without generating any offset in peak-centre position. The instrument monochromator was set do give a wavelength of λ = 1.55Å which allowed measurement of the (311) reflection at 2θ=92°, thus providing an approximately cubic gauge volume.

To allow calculation of stress, strain was measured in three perpendicular directions, namely hoop, radial and axial as indicated on Figure 1. These directions can be assumed to approximate the principle stress directions from the disc geometry. A radial line scan at mid width in combination with an axial line scan at 73mm from the bore made a total of nine measurement points arranged in a cross formation. To balance spatial resolution with count statistics, a gauge volume of 4x4x4 mm^3 was chosen and defined using primary and secondary slits. Data analysis was carried out using in-house software by fitting and subtracting background intensity, followed by a Gaussian fit of the peak itself. This allowed each diffraction peak centre to be expressed in terms of a value of 2θ, which was converted to a value of d-spacing using Bragg's law (Equation 1).

$$\lambda = 2d\sin\theta \tag{1}$$

Strain is calculable from measured d-spacings and a reference (d_0) value using the following relation (Equation 2).

$$\varepsilon = \frac{d^{hkl} - d_0^{hkl}}{d_0^{hkl}} \tag{2}$$

One technique to obtain the stress-free d-spacing (d_0) is to measure individual cubes of material extracted from specific locations in an identically processed specimen at the time of the neutron diffraction experiment. If these cubes are sufficiently small in dimension they may be considered free from macro-stress and allow the true lattice strain to be deduced via Equation 2 [10]. In this study identically processed cubes were not available at the time of the experiment. Instead, cubes were extracted from each sample at a later date and measured in a follow up experiment. The cubes were extracted using Electro-Discharge Machining (EDM) and measured using the strain scanning instrument SALSA at the ILL, Grenoble [11]. To ensure the measured d-spacings from two different instruments could be used to calculate strain, a reference sample of RR1000 powder was measured on each instrument. The measured powder d-spacing was then employed as a scale factor to the data obtained from each instrumental setup.

The water quenching process was known to have set up severe thermal gradients. Consequently, it was expected that a d_0 variation might exist approaching the rim of the disc [12]. In order to compensate for this a cube was extracted from each sample at three radial locations coinciding with neutron measurement points; 45mm, 73mm, and 81mm from the bore centre. The 45mm cube was also used as a d_0 for the 57mm, and 63mm neutron measurement points since they were not affected by near surface d_0 variation.

Upon completion of d_0 measurement, it was possible to calculate strain in the three principal directions, and from this stress using the following relation.

$$\sigma_x = \frac{E_{hkl}}{(1+\nu_{hkl})(1-2\nu_{hkl})}\left[(1-\nu_{hkl})\varepsilon_x + \nu_{hkl}(\varepsilon_y + \varepsilon_z)\right] \quad \text{and} \quad \sigma_y = \ldots etc. \tag{3}$$

Note that in this case, E and v represent the (311) plane specific diffraction elastic constants (DECs) at room temperature, as given in Table 2. The (311) DECs given here were measured previously during an in-situ loading neutron diffraction experiment on the strain scanning instrument Engin-X, (Didcot, UK) [13]. The experiment measured multiple diffraction peaks through increased load in the longitudinal and transverse direction simultaneously. From this data it was possible to calculate the (311) plane specific elastic modulus and Poisson ratio.

Peak position accuracies were calculated in real time during the experiment from the fit uncertainty of each peak using the method outlined by Wimpory [14]. Using this methodology it was possible to adjust count times to account for variations in neutron pathlength depending on measurement position and direction. In doing so a residual stress accuracy of ±50MPa or better was achieved.

Table 2: Ambient temperature properties of RR1000

Material Properties of RR1000	
Young's modulus (bulk)	224 GPa
Poisson ratio (bulk)	0.33
(311) Diffraction elastic constant	203 GPa
(311) Poisson ratio	0.3

2.2 Residual stress analysis using the contour method

The contour method for residual stress characterisation is a destructive technique for obtaining a 2D map of the residual stress normal to a cut surface. The technique consists of three stages, cutting, surface measurement, and analysis. These are shown schematically in Figure 2. The cutting processes (A) causes residual stresses within the component to relax. The resultant deformation of the cut surfaces is representative of the original residual stress distribution (B). Measurement of both deformed surfaces is carried out using either a coordinate measuring machine (CMM) touch probe or laser scanner and the deformed surfaces loaded into an Finite Element (FE) model. Analysis is then carried out by virtually iterating the deformed surface back to planarity (C) and the residual stress field is calculated from the total force required to do this.

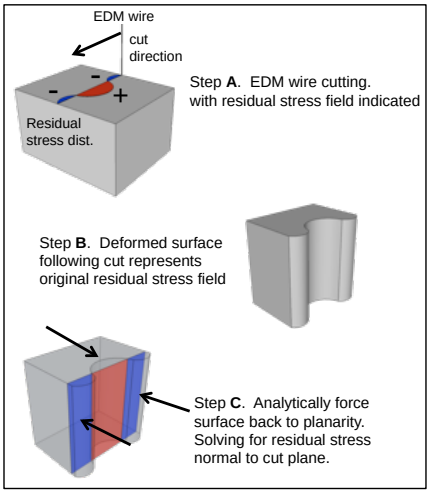

Figure 2: Schematic methodology for obtaining residual stress using the contour method

It is worth noting that two key assumptions are made using this method. First, the relaxation of residual stress and the resulting surface deformation are purely elastic. Second, the cutting process is sufficiently slow and non-aggressive that no additional stresses are introduced during the process. An in-depth description of the contour method can be found in [6].

Due to time and cost constraints only S2 and S3 were measured using the contour method. Each sample was sectioned across the diameter using Electro-Discharge Machining (EDM), with the cut plane aligned to pass through each of the neutron diffraction measurement gauge volumes. The EDM cut was made using so called 'skim cut' settings, which ensure a slow and fine cut that does not contribute to the residual stress state. Each sample was firmly clamped on both sides of the cut to reduce non-symmetric errors which would contribute to the final residual stress calculation [15]. The surface contour of each sample was measured using a Nanofocus confocal laser profilometer at a step size of 100μm. The sample outline was defined as the point at which reflectivity dropped below 80%, thus indicating that the laser had scanned over the edge of the sample; all data points with reflectivity less than 80% were set to a default "mask" value to allow easy identification in later stages of analysis.

Surface contour data sets were manipulated and analysed using a combination of user defined routines in MATLAB [16] and ABAQUS [17]. MATLAB was used to remove "masked" data points and clean outliers. In both cases a 5mm width of contour data was removed in the regions where the wire entered and exited the workpiece to eliminate artifacts generated here [18]. Data from both halves were aligned analytically through minimisation of eigenstrains and the average of both displacements taken. This averaged displacement is then assumed to be exclusively the result of the elastic relaxation of stresses normal to the cut; all other effects including shear and Poisson contribution are averaged out at this stage of the process. Lastly, experimental noise was removed by fitting a bi-variant spline function to the averaged measured surface. Further details on data analysis can be found in [19].

The spline fit represented the initial condition in the model. From this condition the model worked 'backwards' to the final condition of one sample half with a planar surface, and in doing so calculated the stress. The final condition was generated by first importing the sample outline into ABAQUS in order to generate a planar cross-section. The remaining 3D geometry was generated using built-in extrude and cut functions. The part was meshed using quadratic elements with typical length 1mm at the cut surface, which reduced to 3.5mm at the rim of the disc. This allowed relatively short calculation times (60 minutes) whilst maintaining adequate resolution. By assuming elastic isotropy, bulk elastic properties were used (Table 2) and the model was solved using ABAQUS.

The model was subsequently interrogated to obtain residual stress distributions. Two dimensional maps of the stress normal to the surface were generated to visualise the distribution, and undertake first comparisons between S2 and S3. To compare data sets in detail, contour stress data were exported as either radial or axial line scans between any two user-defined points on the sample surface.

3. Process modelling

Model generation

All finite element modelling work was carried out using the Rolls-Royce in-house analysis code 'SCO3' [20]. The problem was defined as a two dimensional cross-section from bore to rim only. This was known to be a valid approximation due to the propensity of all manufacturing processes in this study to generate approximately axi-symmetric residual stress distributions. The geometry was drawn in SCO3 using measured dimensions and meshed using ~1mm length triangular elements throughout the entire cross section (Figure 3).

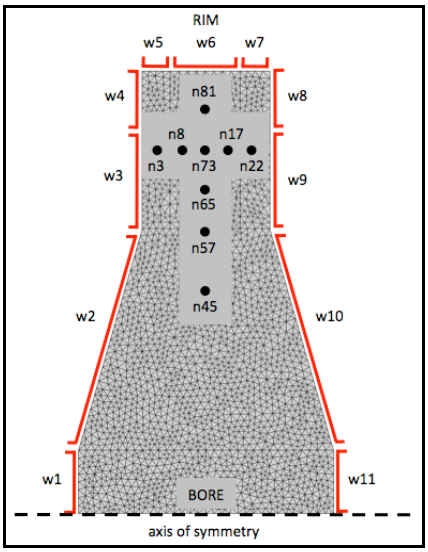

Figure 3: The meshed part as generated in SCO3, complete with neutron diffraction target values ('n' prefix points) and HTC weighting factors (w1-11) indicated.

Quench

The quenching process was modelled through heat extraction at the surfaces of the geometry. Heat extraction comprised of two key stages; firstly, surface radiation during transfer from furnace to quench tank, and secondly, convection currents once immersed in the quench medium. The level of heat extraction during sample transfer was sufficiently low that a simple constant of emissivity could be used to simulate this stage of the quench process. However, once the sample was in contact with water it was necessary to use a heat transfer coefficient (HTC) curve to define the level of heat extraction at any given temperature.

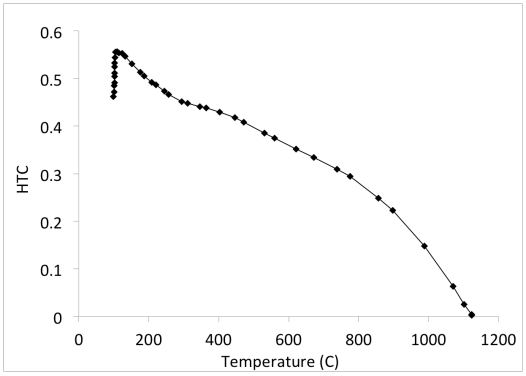

Figure 4: Water quenching HTC curve for a sub-scale forging of the nickel-base superalloy RR1000.

The HTC curve was obtained in a separate investigation using a stainless steel test piece with multiple embedded thermo-couples to record the change in temperature during quench (Figure 4). After taking into account the material properties, the difference in temperature between two proximal thermo-couples was used to derive the level of heat transfer throughout the quenching process and hence the HTC curve of that setup (Figure 4).

The HTC curve was initially applied uniformly to the model as a temperature dependant coefficient of heat extraction on each surface. However, this did not accurately define the process; factors such as sample geometry and orientation when entering the quenching tank caused differential cooling by surface location. To better describe the quenching process the part was broken down into 11 surface regions and a further 'weighting factor' (WF) was employed at each surface to allow cooling rates to vary by location (Figure 3). The method for deriving each WF has been described in later sections as the *inference method*.

Age

Experimentally, S2 and S3 were both water quenched before being aged for sixteen hours at 760°C followed by cooling in still air for a further hour. This process was simulated by interpolating strains from the quench model output into a new model of identical geometry but using ramp points that reflected the thermal history through the ageing process. Stresses were expected to relax via creep during ageing. Therefore, material specific creep rates were added to the simulation process at this stage. The rate of heating and cooling was of sufficiently slow rate during ageing that it was possible to treat the sample as a uniform thermal entity without straying far from the actual manufacturing process.

Machine

The machining process modelled in this investigation was strictly aimed at characterising the re-balancing of residual stresses after material removal, therefore stresses induced from machining itself were in no way considered. This being the case, the simulation of machining was completed by removing the appropriate elements, directly transposing the aged condition (S2) strains onto the new mesh, and then running the model to regain force balance.

In addition, it was assumed that the order in which material was removed did not seriously affect the net residual stress distribution once the machining process was completed [21]. This assumption was tested in a preliminary investigation by modelling material removal on each side first, then both sides at the same time. It was found that the order of material removal made no difference to the final residual stress distribution. It was therefore possible to model the machining sequence by removing all of the relevant elements in one step.

Model execution

The quench model was loaded into an optimisation software package known as 'iSight' [22] to carry out the so called 'inference method' of deriving HTCs. Data from the neutron diffraction study was used to define the target residual stress values in nine locations within the bulk of the sample (Figure 3).

The optimisation process used a 'pointer' algorithm to adjust the eleven weighting factors to minimise the sum of residuals between experimental and modelled residual stresses. However,

weighting factor adjustment was restricted during optimisation to maintain a degree of continuity between neighbouring surfaces. Contained within the optimisation loop was a condition by which the maximum allowable difference between neighbouring weighting factors must be less than two thirds of the average between them**.** Using this method the HTC weighting factors for water quenching were derived as shown in Figure 5. The distribution of weighting factors indicates a rapid cooling at the bore, and near symmetric cooling rate about the centre line (w6). Each derived weighting factor value was multiplied by the HTC curve to give a heat transfer function for each surface region. A final simulation was carried out using this set up to obtain the modelled residual stress following water quench.

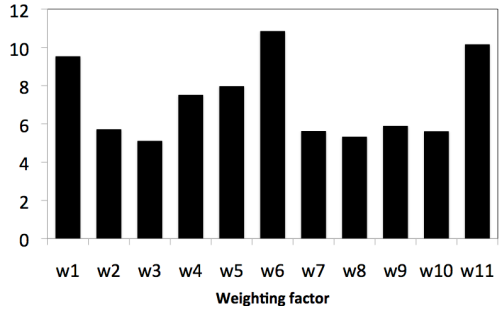

Figure 5: HTC curve weighting factors for the water quenching process as derived using the inference method.

It was recognised that whilst the use of HTC weighting factors would likely achieve high agreement with the experimental residual stress distribution, it potentially masks any underlying issues in the model at the quenching stage. In particular, inaccuracies in thermal or mechanical properties, which would otherwise lead to an incorrect stress prediction, could be at least partially corrected for by the HTC optimisation. To check the HTC inference method was generating realistic levels of cooling throughout the disc, time-temperature curves from the model were compared to measured data from the thermo-couple experiment (Figure 6). Overall the modelled cooling correlates well with the measured data. In the regions close to the rim (P3 & P5), the agreement is high, indicating a well matched cooling rate in proximity to the neutron measurement locations. Closer to the bore, (P1 and P11) the high level of agreement has been maintained, thus the derived HTC weighting factors gave a realistic representation of cooling for the entire sample surface. However in the region deep within the sample bulk the model did not correlate well to the measured cooling (P7). At P7 the model cooled too slowly, yet at the surrounding surface this was not the case (P1&P11).

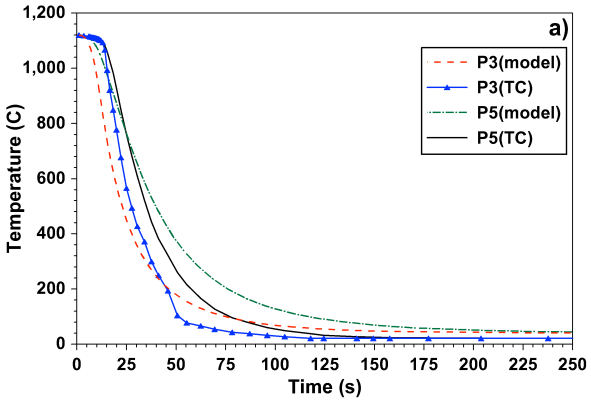

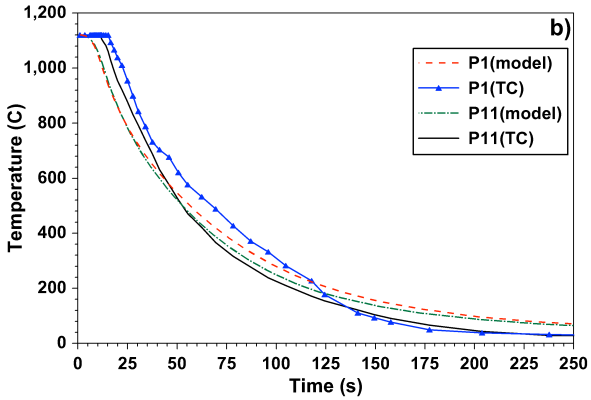

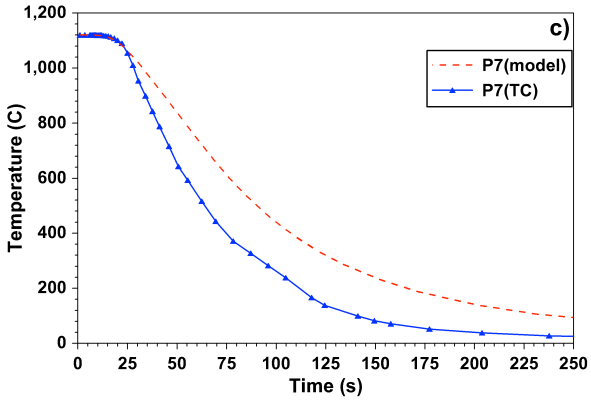

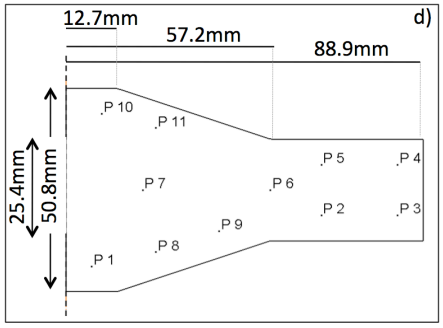

Figure 6: (a-c) Time-temperature history through water quench as obtained by FE simulation (model) and thermo-couple (TC) experiment and d) the thermo-couple locations.

This indicates a possible error in the level of internal conduction rather than surface heat extraction as controlled by the HTC. This being the case, it is possible that the simulated residual stresses will show some disagreement to measured results in the bore region of this disc.

Ageing and machining

Both ageing and machining models were executed without parameter optimisation; thus the simulated residual stress values after age and after machining are representative of the model alone and allow for a more direct comparison of results.

4. Results and Discussion

Neutron diffraction

Figure 7 shows mid-section residual stress evolution in the hoop (a), radial (b) and axial (c) directions using neutron diffraction following quenching, ageing and machining processes. The trends observed following quenching largely follow the expected behaviour. Initial surface cooling over a hot core causes tensile yield in the hoop and radial directions on each face and axial yield around the circumference. After a period of time this process reverses as the core cools and contracts and attempts to draw in the outer surface, thus leaving the surface in biaxial compression and the core in tension [23] .

Following quench, peak tensile stresses are observed in the regions close to the bore in both the hoop and radial directions. Hoop stress falls until reaching the compressive layer at the surface, whereas the radial stress remains tensile throughout. The radial stresses must fall to zero at the free surface of the rim, and the falling trends shown in Figure 7b do indicate that this is likely to be the case. Axially, residual stresses are generally smaller in magnitude when compared to the hoop and radial directions. It is likely that this is the result of a reduced thermal gradient in this direction brought about by the geometry of the disc. The expected compressive axial stress at the disc rim was not captured in this measurement, although a balancing tensile region behind this is just observable. This was due to the need to avoid partial immersion of the large gauge volume, which would have caused the generation of pseudo-strains [7]. Hence the first measurement point is 8mm from the surface.

Beyond this region, moving towards the bore, the stress profile becomes flat, with a roughly constant value of -375MPa. This is a surprising result since disc like geometries are only expected to have significant non-zero axial stress in the rim region, due to edge effects [24]. The issue of non-zero axial stress in disc like geometries has been discussed in the literature [25], and suggested to be the result of residual microstress built up in a particular reflection. Microstresses develop in polycrystalline materials due to elastic and plastic anisotropy. During loading, the stiffness of each grain depends on its orientation to the loading direction, and thus corresponds to the strain accommodated. Upon unloading a residual microstrain develops as neighbouring grains unload strains of a differing magnitude. The stresses resulting from the microstrain are superposed onto that of the bulk [26].

Whilst microstress may be a contributing factor to non-zero axial stress, the Ni (311) reflection is known to exhibit a low sensitivity to this effect, making any contribution small. In addition, the extracted macro-stress free cube will still have contained the microstress field, thus the measured difference between the sample and reference value should be that of the bulk macro-strain only.

In the hoop direction the ageing heat treatment has relaxed tensile stresses in the bulk by up to 450MPa, and compressive stresses at the rim by up to 200MPa. The level of relaxation is reduced at 57mm and 65mm to 280MPa and 40MPa respectively. This indicates that the level of relaxation is likely to be related to the initial residual stress state in terms of level of plasticity, and relaxed via creep [27]. However, at 73mm, ageing appears to have increased the residual stress by at least ~140MPa. Since this is also in strong agreement with S2 contour data at the same location (Figure 8a), it is unlikely that this is an erroneous result in the S2 measurement. Notably, the profile after ageing is quite different to that after quench; a 'peak-like' feature is seen at 65-73mm which was previously not visible.

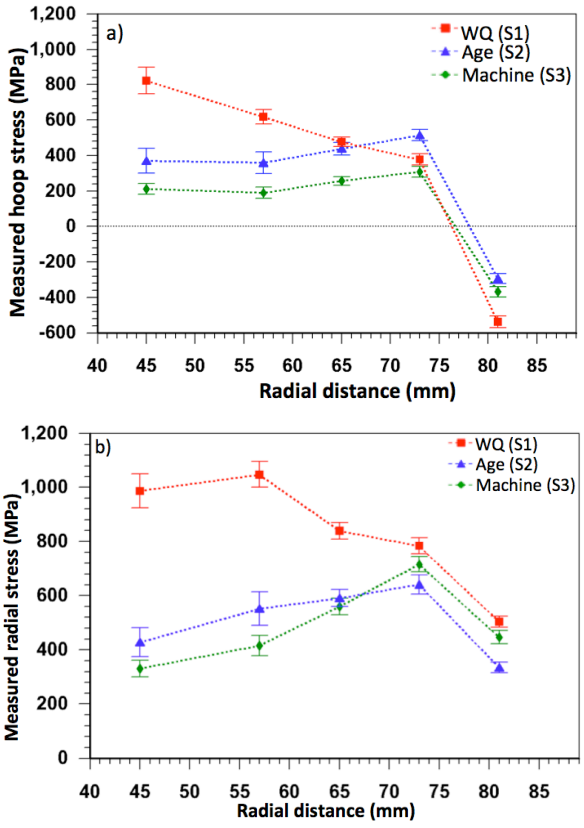

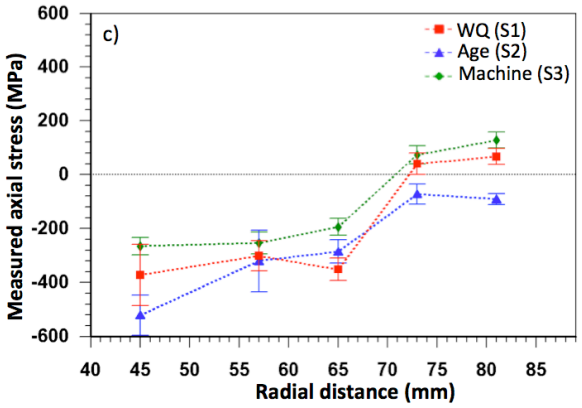

Figure 7: Residual stress as a result of quenching, ageing and machining in the a) hoop, b) radial, and c) axial direction of a sub-scale disc forging. Lines are a guide for the eye only.

Two possibilities for this result offer themselves for consideration. Firstly that the quench process in S2 differed significantly to S1 and that this generated a different initial profile, which remained even after ageing. This is unlikely however since great care in processing was taken to avoid this, and the level of variation to cause this result would be significant. The other possibility is that ageing causes a complex redistribution of residual stress, which has been observed here in the hoop direction. Further investigation of this behaviour could be carried out by re-measuring a quenched sample after ageing to remove any sample to sample variation.

Radially, the ageing heat treatment has relaxed stresses by up to 550MPa in the near bore regions. As was the case in the hoop direction, larger quench stress has again led to increased relaxation during age. However, ageing does not appear to increase the residual stress at any location, although it does still alter the profile.

In comparison the axial direction exhibits very little relaxation from the ageing treatment, which corresponds to the lower initial residual stress from quench. The apparent increase in residual stress following age at 45mm can be discounted once errors are taken into account. The particularly long path length in the axial direction at 45mm in S1 and S2 made larger uncertainty inevitable at this location.

The machining processes have reduced tensile hoop stress in the bulk by 150-200MPa across the 45-73mm line scan. This indicates that material machined from each face (0-57mm radial distance – Figure 1) has caused the bulk residual stress to re-balance. The removal of much of the compressive surface region has caused the tensile region in the sample core to reduce in magnitude in order to maintain equilibrium.

The effect of material removal on the radial stress in the 45-67mm range is much reduced in comparison to the hoop. It is possible therefore that the material removed did not contain such a strong stress field in the radial direction. It appears that the stresses at the 73mm and 81mm locations have increased slightly, despite the material removal being at least 16mm away. This suggests the re-balancing of residual stress following material removal may have far reaching effects.

The Contour Method

Contour method data allowed comparison of residual stress in the hoop direction using a completely independent technique and thus add significant weight to the experimental data set. The results for S2 (age) and S3 (machining operation 1) as measured by the contour method are compared to neutron diffraction data in Figure 8

The contour method **radial line scan** (Figure 8a) of S2 indicates peak tension at the bore and throughout most of the bulk, with a narrow compressive layer at the rim. Following machining (S3) much of this profile is retained although the stress magnitude reduces at almost every location. Notably, even though material was removed in the just ±57mm radius the stress rebalancing extends beyond this range through the whole of the sample. The contour method **axial line scan** (Figure 8b) shows reduction of tensile stresses by ~175MPa at the bore. At the rim (-12.5mm) stress falls by ~300MPa, but at the opposite rim (+12.5mm) they remain the same.

Figure 8a also compares contour data (line) to neutron diffraction data (discrete points) across the **radial line scan**. It is clear that in both S2 and S3 very strong agreement is seen between the two data sets. In the S2 the agreement is marginally worse, particularly close to the bore. This is associated with the larger bore cross-section of S2, which increased the neutron path length at the 45 and 53mm measurement locations. This effect is clearly visible in the larger error bars at these locations in comparison all other measurement points. Close to the rim the contour method data indicates an extremely steep stress gradient is present from 75-89mm, approximately 100MPa/mm. The agreement between neutron and contour method data in this region is therefore subject to an averaging of stresses over the neutron gauge volume. In this case strong agreement was achieved, however steep gradient measurements are usually less reliable when a large gauge is employed.

Some discrepancies exist between the contour method and neutron diffraction data in the **axial line scan**. Whilst a correlation is maintained near the centre line, this is reduced in proximity to the surface. In particular the neutron diffraction data at ±9.5mm in both samples is more compressive than that measured using the contour method.

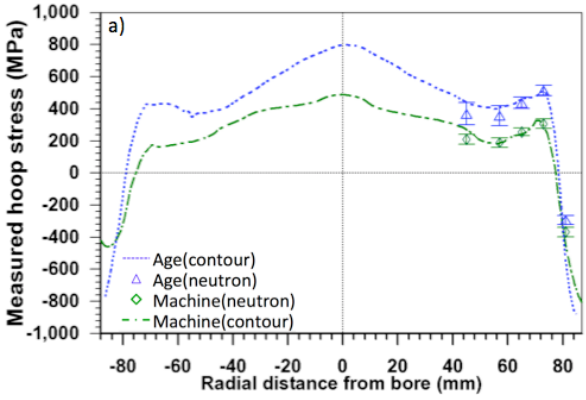

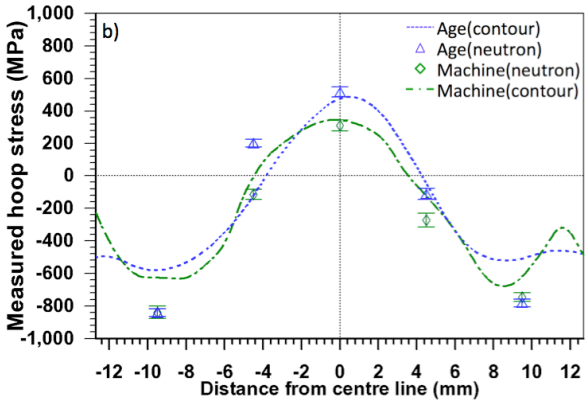

Figure 8: Hoop residual stress distributions over a) a radial line scan at the centre thickness and b) an axial line scan at 73mm radial distance, in S2 and S3 as measured by the contour method and by neutron diffraction.

The trends observed in the contour data are highly symmetric about the bore and about the centre thickness, particularly in the aged sample (S2). From this result it is inferred that the quench and ageing heat treatments were carried out reasonably homogeneously at each surface. The only exception to this trend is seen in S3 at the rim; from -80mm to the rim (-89mm) the residual stress appears to level off and then marginally increase. Since this profile is not observed at the other rim, or at all in the other sample it is suspected that this result be anomalous. The wire cutting direction was recorded and it is known that at this location the wire was leaving the sample. It is possible that as the wire exited the sample, it could have moved in the clamp, or that some transient effect of the cutting process may have affected the surface contour at this position.

Finite element modelling

Simulated residual stress profiles across the centre-thickness radius, have been modelled in the hoop, radial and axial directions (Figure 9). Each profile has been compared to all available experimental data.

In the hoop direction, the simulated quench stress matches well with experimental data at the neutron diffraction locations. At the bore, simulated quench stresses reach 1400MPa, which exceeds yield in this material. However, once the other two directions are taken into account, the Von-Mises stress is found to peak at ~1100MPa at the bore; below 0.2% yield. Following age, the simulated data is compared to both the contour and neutron diffraction data sets. The contour and neutron data clearly correlate very strongly, but this can only be said of the model at the 45, 57 and 81mm locations. At 65-73mm the model under-predicts the post-age stress in such a way as to miss a peak-like feature in the experimental data. At the bore and the rim the model also under-predicts the residual stress in comparison to experimental data. Such a discrepancy may be the result of the modelled creep behaviour, which is currently only well defined in a post age microstructure rather than as-quenched.

The material removal following machining was predicted to reduce stresses in the bore region, and marginally increase them in the rim region. The experimental data agrees with this overall trend, although localised variations captured by the neutron and contour techniques are not visible in the simulated data. At the bore the model still under-predicts the magnitude of residual stress, although the level of relaxation from S2 to S3 is well matched. Interestingly, at the 73mm location both S2 and S3 experimentally exhibit a similar peak-like feature not observed in the model. Since the two samples were measured identically but independently, the measured feature at 73mm seems to be real. Clearly this is not observed in the simulated data which points to an issue in the ageing model. The fact that the machining model did not match this result in S3 is not surprising, since the model used the as-aged model result as a starting point.

The radial stresses (Figure 9b) are generally well predicted throughout the processing stages. In the as-quenched condition (S1), the measured and simulated data sets follow the same trend, although discrepancy is clearly observed at the 45mm and 65mm locations. Without additional data it is not clear whether this is due to an issue with the experimental or simulated data. The ageing process is predicted to reduce residual stress by as much as 750MPa at the bore, and the nearest neutron measurement point in S2 indicates this to be an accurate prediction. Overall, agreement in the aged condition is high with the exception of the 73mm location, which is under-predicted in a similar way to that observed in the hoop direction. Given that quenched stresses are well predicted in both hoop and radial directions, it would appear that stress relaxation through ageing is not well simulated in this region of the disc.

Machining is predicted to reduce radial stress exclusively in regions from which material has been removed, i.e. over 0-57mm radial distance. Experimentally this is mostly borne out, as only the 45mm and 57mm data points show a reduction in stress following machining and the 65mm location shows no change. At 73mm and 81mm, the model predicts no change following machining whereas the neutron data showed a small increase in stress. This indicates stress re-distribution following material removal may extend beyond the localised region, although this is not predicted in the radial direction.

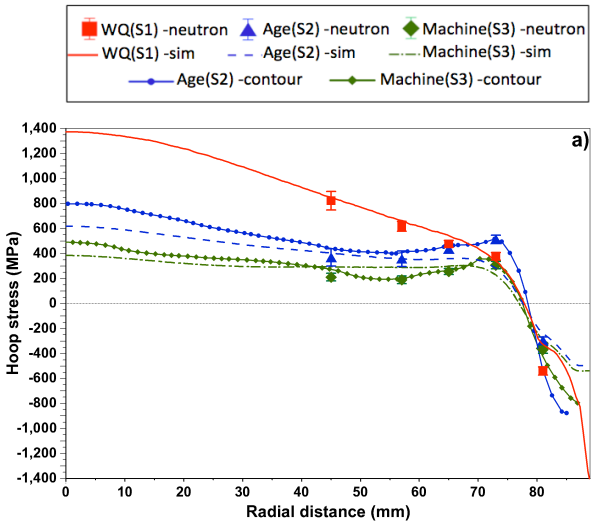

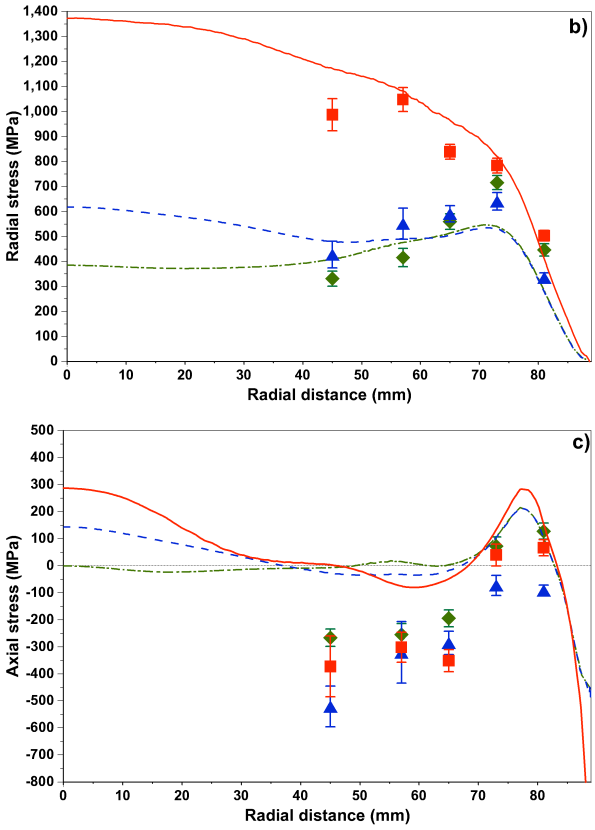

Figure 9: Simulated and experimental residual stress distributions over a radial line scan in the a) hoop b) radial and c) axial stress directions.

In the axial direction the simulated and experimental data sets generally show quite different trends. In the as-quenched condition the two datasets match only at 73mm and 81mm radial distance; the region of balancing tensile stress behind the strongly compressive surface. The agreement here is relatively weak, but stress gradients around this feature are high. It is likely that neutron diffraction gauge volume averaging, due to spatial resolution of ~6mm along the scattering vector, has reduced agreement. Since the neutron measurements were not made closer than 8mm to the rim surface it is not possible to comment whether the modelled surface compressive region would have also been observed experimentally. However, since the tensile feature associated with the compressive surface is visible experimentally, it is reasonable to assume that the predicted trend at the surface is realistic.

From 0-67mm radial distance, the predicted and measured quenched stresses are markedly different in magnitude. Whilst the model predicts tension at the bore slowly falling to near zero at 45mm radial distance, the experimental data is strongly compressive over the 45-67mm region. The same discrepancy is seen here in both the aged and machined samples, which suggests this result is not a measurement, or model user-setup error. In earlier discussion it was highlighted that residual microstresses are unlikely to be the cause of the experimental values seen here. Ideally, more experimental data would be available from 0-45mm radial distance to fully characterise this behaviour, however neutron pathlengths within the thicker cross-section were prohibitively long.

Ageing is predicted to relax bore tensile stress by ~120MPa, rim compressive stress by ~300MPa, and the tensile peak (73-81mm) by ~100MPa. Experimental data was not obtained for the bore/rim regions due to pathlength, and near surface issues in the neutron diffraction experiment. At the tensile peak the measured change in stress, following age, is felt to be unrealistic in magnitude. Given the low axial stress in this region it would be expected that neither ageing nor machining would have a large impact on stress relaxation at the 73-81mm measurements locations. S1 and S3 agree with the expected behaviour, as does the model, it is therefore particularly surprising that S2 does not. Since peak fitting errors are low close to the rim, and a more than adequate d_0 characterisation was carried out, it is illogical to cite a measurement error in this instance. Given that the discrepancy is relatively minor, and within a region of rapidly changing stresses by virtue of being close to the rim; it is felt that minor process variations are likely to have generated this result.

The machining operation removed material to reduce the axial cross-section over the 0-57mm radial distance. The simulated results (Figure 9c) indicate that removal of this material reduces the cross-section to the point that axial stresses fall from ~100MPa to zero for much of the bore region. No experimental data was obtained for the 0-45mm region, but from the data obtained beyond this point it appears unlikely that the axial stress datasets would agree here. In the regions were experimental data was obtained (45-81mm), the absolute values in S3 differ to the simulation, most likely due to the original discrepancy in S1. However the negligible level of relaxation, following material removal, does approximately correlate in both the simulated and experimental data.

5. Conclusions

In this article, residual stresses in three sub-scale forging geometries of the nickel superalloy RR1000 have been characterised following key manufacturing processes. Experimental datasets obtained using the neutron diffraction and contour method techniques have been compared to finite element modelled predictions. Based on the results obtained, the following conclusions can be drawn.

1. It was possible to use neutron diffraction to map the generation and subsequent redistribution of bulk residual stress in sub-scale forgings through the quenching, ageing, and machining processes.
2. In the forging geometries measured, hoop and radial stresses were significantly larger than axial stresses post quench. As a consequence, the ageing process had the greatest impact on residual stress relaxation in the hoop and radial directions.
3. The contour method of measuring residual stress was demonstrated to agree very strongly with the neutron diffraction technique in the as-aged and machined conditions. The full diameter stress profiles generated by the contour method highlighted the strongly axi-symmetric stress distribution in the hoop direction.
4. Thermo-couple trials were used to derive a heat transfer coefficient curve for water quenching. The curve was scaled up at each surface using the inference method to match measured and simulated bulk residual stress values.

The subsequent modelled cooling rates were found to match well with the original thermo-couple trial data, thus validating this approach.

5. Finite element modelling predictions generally correlated well with experimental data; a number of observations were made:
   a. Quench stresses were very well predicted in the hoop direction across the centre line scan. In the radial direction some discrepancy was visible at the 45mm and 65mm measurement locations.
   b. The predicted hoop stress post age differed from both, the contour and neutron diffraction data, in a number of locations. This was also observed to a lesser extent in the radial direction. A possible source of error was identified in the currently available creep data.
   c. The residual stress following machining was well predicted in the hoop direction, showing stronger agreement with both the neutron and contour data. At the bore the stresses were under-predicted by ~100MPa, but the level of relaxation was well matched to experimental data.
   d. In the radial direction the effect of machining was largely localised to the region of material removal. Measured values did indicate some stress redistribution beyond the localised region, which was not predicted in the model.
   e. The axial direction showed the worst overall agreement between simulated and measured residual stress in every sample. Away from the rim the model predicted near zero stresses whereas the measured data indicated compression up to 400MPa. However, both the simulated and measured results indicated the ageing and machining processes had little effect on the residual stress profile in this direction.

The next stages of this research should be targeted towards understanding the observed discrepancies between the measured and simulated values presented here. In particular the relaxation of residual stresses during an ageing heat treatment, which resulted in differing profiles in the predicted and measured results in the hoop and radial direction. To facilitate this, the use of in-situ ageing measurement capabilities may be required to reduce sample processing variations and therefore to fine-tune the ageing model. The poor agreement in the axial direction is highly significant since stresses are of very different magnitude and the opposite sign. Such a result requires more experimental data in the bore region to fully characterise this issue. Finally, in order for quenching simulations to be well tested and improved, it is necessary for the HTC curve to be defined independently beforehand. Once this has been achieved, detailed comparisons can be made between the measured and predicted stress profiles following quenching. In the long term, this will lead to an improved capability in forward-predicting residual stresses throughout manufacture.

ACKNOWLEDGMENTS

This work forms part of an EngD project, sponsored by the Engineering and Physical Science Research Council (EPSRC), UK, with additional support from by Rolls-Royce plc., and working in collaboration with ATI Ladish Forgings, USA. The authors would like to acknowledge the contributions of Rob Mitchell and Benedict Grant, Rolls-Royce plc., Robert Goetz and John Matlik, Rolls-Royce Corporation, Indianapolis, USA. Joe Lemsky, ATI Ladish Forgings. For the provision of neutron beam time: The ILL (Grenoble, France), the FRM2 (Munich, Germany) and the NMI3 neutron and muon research fund. For technical assistance and discussion, Richard Moat (formerly University of Manchester and now Open University), Philipp Frankel, and Naveed Iqbal (University of Manchester).

REFERENCES

[1] Hardy MC, Zirbel B, Shen G, Shankar R. Developing damage tolerance and creep resistance in a high strength nickel alloy for disc applications. Superalloys 2004:83-92.

[2] Ball DL, Tom BK, Bucci RJ, James MA. Toward Understanding the Impact of Bulk Residual Stress on the Life, Weight and Cost of Primary Aircraft Structure. Residual Stress Summit. Tahoe City, CA, 2010.

[3] Schajer GS. Residual Stresses: Measurement by Destructive Testing. Encyclopedia of Materials: Science and Technology. Elsevier, 2001. p.8152-8158.

[4] Hutchings MT, Withers PJ, Holden TM, Lorentzen T. Introduction to the Characterization of Residual Stress by Neutron Diffraction. London: Taylor and Francis, 2005.

[5] Lodini A. Analysis of Residual Stress by Diffraction using Neutron and Synchrotron Radiation. London: Taylor and Francis, 2003.

[6] Prime MB. Cross-sectional Mapping of Residual Stresses by Measuring the Surface Contour After a Cut. Transactions of the ASME 2001;123:162-168.

[7] Withers PJ, Bhadeshia HKDH. Residual Stress Part 1 - Measurement Techniques. Materials Science and Technology 2001;17:355-365.

[8] Hofmann M, Schneider R, Seidl GA, Rebelo-Kornmeier J, Wimpory RC, Garbe U, Brokmeier H-G. The new materials science diffractometer STRESS-SPEC at FRM-II. Physica B 2006:1035-1037.

[9] Stone HJ, Holden TM, Reed RC. Determination of the plane specific elastic constants of waspaloy using neutron diffraction. Scripta Materialia 1999;40:353-358.

[10] Withers PJ, Preuss M, Steuwer A, Pang JWL. Methods for obtaining the strain-free lattice parameter when using diffraction to determine residual stress. Journal of applied crystallography 2007;40:891-904.

[11] Pirling T, Bruno G, Withers PJ. SALSA--A new instrument for strain imaging in engineering materials and components. Materials Science and Engineering: A 2006;437:139-144.

[12] Rolph J, Iqbal N, Preuss M, Hofmann M, Evans A, Ganesan M. The Effect of d0 Reference Value on a Neutron Diffraction Study of Residual Stress in a Gamma/Gamma Prime Nickel-base Superalloy. (Submission in process) 2012.

[13] Grant B, Elisabeth K, Preuss M, Quinta da Fonseca J, Daymond MR. The Effect of Lattice Misfit on Deformation Mechanisms at High Temperature. Advanced Materials Research 2011;278:144-149.

[14] Wimpory RC, Ohms C, Hofmann M, Schneider R, Youtsos AG. Statistical Analysis of residual stress determinations using neutron diffraction. International Journal of Pressure Vessels and Piping 2009:48-62.

[15] Prime MB, Kastengren AL. The Contour Method Cutting Assumption: Error Minimization and Correction. Proceedings of the SEM Annual Conference & Exposition on Experimental and Applied Mechanics Indianapolis 2010.

[16] Mathworks. MATLAB 7.10. Natick, MA., 2010.

[17] SIMULIA. ABAQUS Software. Rising Sun Mills, 166 Valley Street, Providence, RI., 2011.
[18] Frankel PG. Residual Stresses in Aerospace Components. Material Science, vol. EngD. Manchester: University of Manchester, 2008. p.38-40.
[19] Prime MB, Sebring RJ, Edwards JM, Hughes DJ, Webster PJ. Laser surface contouring and spline data smoothing for residual stress measurement. Experimental Mechanics 2004;44:176-184.
[20] Bibby GP. Compressor Engineering SCO3 Radial Displacement Plot Facility. Rolls-Royce, 1998.
[21] Hesketh G, Goetz R, Matlik J, Shen G. Disc Residual Stress Modelling. Rolls-Royce plc, 2011.
[22] SIMULIA. iSight Optimization software. Rising Sun Mills, 166 Valley Street, Providence, RI., 2011.
[23] Dye D, Conlon KT, Reed RC. Characterization and Modeling of Quenching-Induced Residual Stresses in the Nickel-Based Superalloy IN718. Metallurgical and Materials Transactions A 2004;35A:1703-1713.
[24] Fletcher AJ, Lewis C. Effect of free edge on thermal stresses in quenched steel plates. Materials Science and Technology 1985;1:780-785.
[25] Cihak U, Staron P, Clemens H, Homeyer J, Stockinger M, Tockner J. Characterization of residual stresses in turbine discs by neutron and high-energy X-ray diffraction and comparison to finite element modeling. Materials Science and Engineering A 2006;437:75-82.
[26] Dye D, Stone HJ, Reed RC. Intergranular and interphase microstresses. Current Opinion in Solid State Materials Science 5 2001:31-37.
[27] Zhou Z, Gill AS, Qian D, Mannava SR, Langer K, Wen Y, Vasudevan VK. A finite element study of thermal relaxation of residual stress in laser shock peened IN718 superalloy. International Journal of Impact Engineering 2011;38:590-596.